Inelastic neutron scattering, lattice dynamics, and high-pressure phase stability of zircon-structured lanthanide orthophosphates

Preyoshi P. Bose,[1] R. Mittal,[1] S. L. Chaplot,[1] C.-K. Loong,[2] and L. A. Boatner[3]
[1]*Solid State Physics Division, Bhabha Atomic Research Centre, Trombay, Mumbai 400085, India*
[2]*School of Physics and Engineering, Sun Yat-Sen University, Guangzhou 510275, China*
[3]*Oak Ridge National Laboratory, Oak Ridge, Tennessee 37831, USA*
(Received 25 June 2010; revised manuscript received 30 July 2010; published 22 September 2010)

Inelastic neutron-scattering experiments and lattice-dynamical calculations are reported on a series of rare-earth orthophosphates RPO_4 (R=Tm, Er, Ho, and Tb). The experimental phonon spectra for the compounds are in good agreement with our model calculations. The lattice-dynamical model is found useful for the calculation of various thermodynamic properties such as the lattice specific heat, thermal expansion, and equation of state of these compounds. The RPO_4 compounds are known to transform to the scheelite (body-centered tetragonal, $I4_1/a$) or monoclinic phase ($P2_1/n$) at high pressures. Our calculations show that while the scheelite phase stabilizes at high pressure due to its lower volume, the monoclinic phase may occur as an intermediate phase depending on the ionic size of the R atom. The latter phase is stabilized at higher temperature (at high pressure) due to its high vibrational entropy. A pressure-temperature phase diagram is proposed.

DOI: 10.1103/PhysRevB.82.094309 PACS number(s): 78.70.Nx, 63.20.−e, 65.40.−b

I. INTRODUCTION

Orthophosphates formed by mixed lanthanides are of particular interest since a relatively high concentration of various lanthanides is present in the waste resulting from reprocessing of light water reactor spent fuel in the recent years. The main potential applications include host matrices for immobilization of certain types of radioactive wastes,[1,2] solid ion conductors,[3] and multilayered weak-bonded ceramic composites.[4] The pure rare-earth lanthanide orthophosphates (RPO_4) are structurally divided into two classes: the first half of the series (La-Gd) has monoclinic structure with space group $P2_1/n$ while the second half of the series (Tb, Lu, Y, and Sc) has the tetragonal zircon structure with space group $I4_1/amd$. Stabilization of RPO_4 in the zircon or monoclinic structure is effected by the size of the R-site cation. In both the structure types, phosphorus is in fourfold coordination with oxygen forming isolated tetrahedra. The rare-earth atom is in eightfold coordination in the zircon structure, while the monoclinic modification, allowing a dense packing of oxygen atoms, the coordination of the R-site cation becomes ninefold. The excellent refractory properties at high temperatures, high radiation-damage resistance, and good chemical stabilities have prompted systematic investigations by many workers.[5] These include studies of optical,[6] transport,[7] phonon,[8,9] and thermochemical properties,[10–12] the variation in thermal and mechanical properties with respect to the rare-earth constitutions[13,14] and radiation effects[15,16] by various theoretical and experimental techniques.[17–20] However, we are not aware of a systematic assessment of the phonon spectra and the associated thermodynamic properties and possible phase transformations in the heavy lanthanide orthophosphates.

With regard to the zircon versus other distorted structures, high-pressure Raman spectroscopic and x-ray diffraction studies have also been reported[21–25] for rare-earth phosphates and vanadates. Zircon-structured compounds are known to transform to the scheelite phase (body-centered tetragonal, $I4_1/a$) and monoclinic phase ($P2_1/n$) at high pressure and temperature. Zircon-structured $YbPO_4$ and $LuPO_4$ have been found to undergo phase transitions[23] to a tetragonal scheelite ($I4_1/a$, $Z=2$) structure at 22 GPa and 19 GPa, respectively. X-ray diffraction studies[22] performed on $ScPO_4$ and YPO_4 under nonhydrostatic conditions showed zircon-to-scheelite phase transition. However, more recently, high-pressure x-ray diffraction measurements on orthophosphates such as YPO_4 and $ErPO_4$ up to 30 GPa using neon as pressure-transmitting medium showed a zircon-to-monoclinic ($P2_1/n$, $Z=4$) phase transition at 19.7 GPa and 17.3 GPa, respectively. The phase transition is found to be reversible upon decompression. Raman measurements for $TbPO_4$ carried out up to about 15 GPa indicate a transformation[24] from zircon to a lower crystal symmetry phase, most likely monoclinic, at around 9.5 GPa. Further, $TmPO_4$ shows transformation to a monoclinic phase with increasing pressure at 16 GPa.

Earlier we have reported lattice-dynamical studies and neutron-scattering measurements for zircon-structured silicates[26,27] ($MSiO_4$, M=Zr, Hf, U, and Th) and phosphates[9] ($LuPO_4$ and $YbPO_4$). We have shown that the stability of the monoclinic phase in zircon-structured compounds is related to the ionic size of the M atom. The monoclinic phase is found to be unstable for the silicates with the smaller Hf and U ions and it becomes stable, for example, with the larger Th ion. Now we have investigated rare-earth phosphates to understand the thermodynamic behavior of RPO_4 (R=Tm, Er, Ho, and Tb). The potential parameters for $LuPO_4$ and $YbPO_4$ (Ref. 9) are used as the starting point for calculations of these compounds. The calculated phonon densities of states agree well with neutron spectroscopic measurements carried out on polycrystalline samples of these compounds. A transferable interatomic potential model is used to study high-pressure phase transitions. The calculated phase diagrams are in fair agreement with the reported experimental observations.

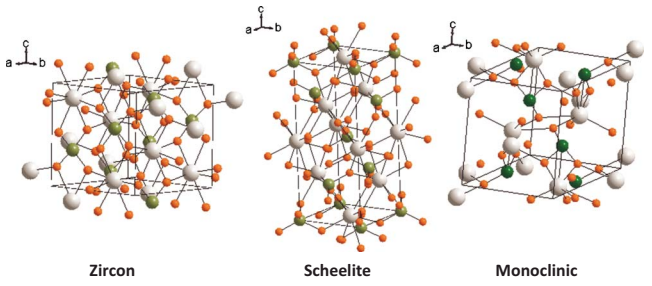

FIG. 1. (Color online) Ball and stick representation of the zircon (space group $I4_1/amd$), scheelite ($I4_1/a$) and monoclinic ($P2_1/n$) phases of RPO_4 (R=Tm, Er, Ho, and Tb). The solid circles denote R, P, and O atoms in decreasing order of size.

II. STRUCTURE

The zircon phase belongs to a tetragonal structure (space group $I4_1/amd$, $Z=2$) and contains 2 f.u./primitive cell. The R and P atoms reside in special Wyckoff sites 4a (0, 3/4, 1/8) and 4b (0, 1/4, 3/8), respectively. The R atoms are eightfold coordinated while P atoms are fourfold coordinated to O atoms. All of the O atoms reside in the 16h $(0,v,w)$ site. The high-pressure scheelite structure belongs to body-centered tetragonal structure with space group $I4_1/a$ and 2 f.u./primitive cell. The R and P atoms reside in special Wyckoff sites 8d (0, 1/4, 5/8) and 8c (0, 1/4, 1/8), respectively. The R atoms are eightfold coordinated and the P atoms are fourfold coordinated to O atoms. All the O atoms reside in the 16f (u,v,w) site. While going from zircon-to-scheelite structure the unit cell is doubled along the c axis. The polyhedra formed in both the zircon and scheelite phases are all regular. The monoclinic structure belongs to the space group $P2_1/n$. The cell contains 4 f.u. for a total of 24 atoms. All the R, P, and O atoms in the unit cell reside in the 4e (u,v,w) sites according to the Wyckoff notation. R and P atoms are in ninefold and fourfold coordinated to O atoms, respectively. In the monoclinic structure the R atoms have ninefold coordination and form distorted polyhedra due to the inclusion of the ninth oxygen atom in the regular polyhedra. The crystal structures of all the phases are shown in Fig. 1.

III. EXPERIMENTAL

The inelastic neutron-scattering measurements for $TmPO_4$, $ErPO_4$, $HoPO_4$, and $TbPO_4$ are carried out using the high-resolution medium-energy chopper spectrometer at the Intense Pulsed Neutron Source of Argonne National Laboratory. High-purity, zircon-structured polycrystalline samples, prepared by a precipitation method described elsewhere,[28] were placed inside a sealed aluminum container. The data have been collected with incident neutron energy of 200 meV over a wide range of scattering angles, corresponding to the momentum transfers Q from 11 to 20 Å^{-1}. These spectra summed over Q represent a close appropriation of the phonon density of states and contain minimal contribution from magnetic scattering of the rare-earth ions due to the vanishing magnetic form factor at high Q. In order to reduce the multiphonon scattering the measurements are carried out at 15 K.

IV. LATTICE-DYNAMICAL CALCULATIONS

Our lattice-dynamical calculations involve semiempirical interatomic potential consisting of the long-range Coulombic and short-range terms. This approach allows us to take into consideration the vibrational entropy contribution to the Gibbs free energy, which is normally not included in *ab initio* calculations. The contribution is found to be important while calculating the zircon-to-monoclinic phase transition as discussed later in Sec. V C. The interatomic potential is given by the following expression:

$$V(r) = \frac{e^2}{4\pi\varepsilon_0}\frac{Z(k)Z(k')}{r} + a\exp\left(\frac{-br}{R(k)+R(k')}\right) - \frac{C}{r^6} - D\exp\left[\frac{-n(r-r_0)^2}{2r}\right], \quad (1)$$

where "r" is the separation between the atoms of type k and k'. $R(k)$ and $Z(k)$ refer to effective radii and charge parameters of the atom of type k, respectively. C is an empirical parameter, $a=1822$ eV and $b=12.364$. The covalent nature of the P-O bond is accounted for by including a bond-stretching term as given by the third term in Eq. (1). The polarizability of oxygen atoms is included in the frame work of the shell model.[29,30] Parameters of the potential are determined such that the calculated crystal structure in the zircon phase of the compounds obtained from free-energy minimization at $T=0$ K is close to that determined using diffraction experiments. Further, the calculated phonon frequencies have real values for all the wave vectors in the Brillouin zone. The potential thus satisfies the static and dynamic equilibrium conditions of the crystal system. The interatomic potential model is further exploited for the calculation of crystal structures at high pressures by minimization of the free energy at $T=0$ K with respect to the lattice-parameter and atomic-position variations, while keeping the space-group symmetry unchanged. The good agreement between the calculated and experimental thermodynamic properties (as discussed later) and phase diagrams indicate that the transferable model is quite reasonable.

The effective radius parameter for the short-range interactions in the interatomic potential may be expected to be proportional to the ionic radius for similar atoms in similar environment. In our earlier work on $MSiO_4$, we found that the radius of the atom at the M site played an important role in determining the high-pressure phase. The potential parameters for $LuPO_4$ (Ref. 9) are used as the starting point for calculation of RPO_4. The effective radii parameters of the rare-earth atoms in the short ranged are optimized to reproduce the experimentally observed phase transitions. Further details are discussed in Sec. V C. The optimized values are $R(\mathrm{Tm})=2.110$ Å, $R(\mathrm{Er})=2.130$ Å, $R(\mathrm{Ho})=2.155$ Å, and $R(\mathrm{Tb})=2.208$ Å. The potential satisfactorily reproduces the available experimental values of the lattice parameters and fractional atomic coordinates in the zircon phase of the various phosphates (Table I).

The phase diagrams of compounds are calculated by comparing the Gibbs free energies of the compounds in various phases. The Gibbs free energy of the nth phase is given by

TABLE I. Comparison between calculated structural parameters (at $T=0$ K) of zircon, monoclinic and scheelite phases of $TmPO_4$, $ErPO_4$, $HoPO_4$, and $TbPO_4$ and available experimental data (Refs. 28–31). The experimental zircon phase structural parameters of $TmPO_4$, $ErPO_4$, and $TbPO_4$ are at ambient temperature and pressure while for $HoPO_4$ the data is at 12 K and ambient pressure. For zircon structure (body-centered tetragonal, $I4_1/amd$) the R (Er, Ho, Tb, and Tm), P, and O atoms are located at $4a$ (0, 0.75, 0.125), $4b$ (0, 0.25, 0.375), and $16h$ $(0,v,w)$, respectively. For monoclinic structure (space group $P2_1/n$) the R, P, and O atoms are located at $4e$ (u,v,w). For scheelite structure (body-centered tetragonal, $I4_1/a$) the R, P, and O atoms are located at $8d$ (0, 0.25, 0.625), $8c$ (0, 0.25, 0.125), and $16f$ (u,v,w), respectively.

	Experimental (Ref. 32) $TmPO_4$ (zircon) 0 GPa, 300 K	Calculated $TmPO_4$ (zircon) 0 GPa, 0 K	Calculated $TmPO_4$ (scheelite) 0 GPa, 0 K	Experimental (Ref. 32) $ErPO_4$ (zircon) 0 GPa, 300 K	Calculated $ErPO_4$ (zircon) 0 GPa, 0 K	Calculated $ErPO_4$ (scheelite) 0 GPa, 0 K
a (Å)	6.839	6.76	4.82	6.860	6.79	4.83
c (Å)	5.986	6.20	11.35	6.003	6.21	11.41
u		0	0.271		0	0.271
v		0.164	0.645		0.164	0.646
w		0.355	0.559		0.356	0.559
Volume/primitive cell (Å^3)	140.0	141.8	131.8	141.2	143.3	133.1

	Experimental (Ref. 33) $HoPO_4$ (zircon) 0 GPa, 12 K	Calculated $HoPO_4$ (zircon) 0 GPa, 0 K	Calculated $HoPO_4$ (scheelite) 0 GPa, 0 K	Experimental (Ref. 34) $TbPO_4$ (zircon) 0 GPa, 300 K	Calculated $TbPO_4$ (zircon) 0 GPa, 0 K	Calculated $TbPO_4$ (scheelite) 0 GPa, 0 K
a (Å)	6.833	6.82	4.85	6.941	6.90	6.89
c (Å)	6.0166	6.24	11.47	6.070	6.29	11.63
u		0	0.272		0	0.273
v		0.163	0.648		0.162	0.652
w		0.356	0.559		0.358	0.560
Volume/primitive cell (Å^3)	140.4	145.4	134.9	146.2	149.8	139.0

	Calculated $TmPO_4$ (monoclinic) 11 GPa, 0 K	Calculated $ErPO_4$ (monoclinic) 10 GPa, 0 K	Calculated $HoPO_4$ (monoclinic) 10 GPa, 0 K	Calculated $TbPO_4$ (monoclinic) 10 GPa, 0 K
a (Å)	6.44	6.46	6.49	6.55
b (Å)	6.58	6.60	6.63	6.69
c (Å)	6.45	6.47	6.49	6.53
β (deg)	105.3	105.2	105.1	105.0
Volume (Å^3)	264	266	270	277

	Calculated ($TmPO_4$) (monoclinic) 11 GPa, 0 K			Calculated ($ErPO_4$) (monoclinic) 10 GPa, 0 K			Calculated ($HoPO_4$) (monoclinic) 10 GPa, 0 K			Calculated ($TbPO_4$) (monoclinic) 10 GPa, 0 K		
	u	v	w	u	v	w	u	v	w	u	v	w
R	0.258	0.156	0.088	0.258	0.156	0.089	0.258	0.157	0.089	0.259	0.158	0.089
P	0.144	0.157	0.588	0.144	0.157	0.588	0.146	0.158	0.588	0.148	0.158	0.588
O1	0.249	0.325	0.497	0.249	0.324	0.497	0.250	0.324	0.496	0.251	0.323	0.496
O2	0.260	0.099	0.764	0.262	0.100	0.763	0.262	0.100	0.762	0.264	0.101	0.760
O3	0.105	0.206	0.671	0.106	0.206	0.670	0.108	0.207	0.670	0.110	0.207	0.670
O4	0.227	0.506	0.048	0.227	0.507	0.048	0.227	0.508	0.048	0.228	0.510	0.047

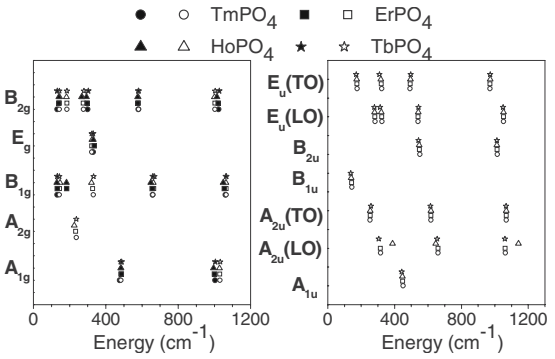

FIG. 2. The comparison between the calculated (T=0 K) and experimental (Ref. 13, T=300 K) zone-center phonon frequencies for zircon phase of RPO_4 (R=Tm, Er, Ho, and Tb). The calculated infrared-active modes are also shown. The closed and open symbols represent the experimental and calculated frequencies in the order stated. The frequencies are plotted in the order of $TmPO_4$, $ErPO_4$, $HoPO_4$, and $TbPO_4$ from below (1 cm^{-1}=0.124 meV).

$$G_n = \phi_n + PV_n - TS_n, \tag{2}$$

where, ϕ_n, V_n, and S_n, respectively, relate to internal energy, lattice volume and vibrational entropy of the nth phase. The Gibbs free energy of various phases is compared at different pressures for a particular temperature. Thus we obtain the phase diagram.

V. RESULTS AND DISCUSSION

A. Phonon density of states

The calculated Raman and IR zone-center phonon frequencies for all compounds in the zircon phase are shown in Fig. 2. The calculated Raman modes are in good agreement with the experimental data,[20] i.e., within a 4% deviation. The experimental data for the IR modes are not available. The effect of mass and radii variation in the R atom is not significant in the Raman-active modes whereas A_{2u} and E_u modes show slight effect.

The calculated partial phonon density of state in the zircon phase is shown in Fig. 3. From the partial density of states we observe that the R atoms contribute only up to 50 meV. The P and O atoms span the entire spectral range of 0–145 meV. The modes above 115 meV are purely due to P-O stretching vibrations. The partial density of states is further used to calculate the neutron-weighted phonon density of states (Fig. 3) via the relation.

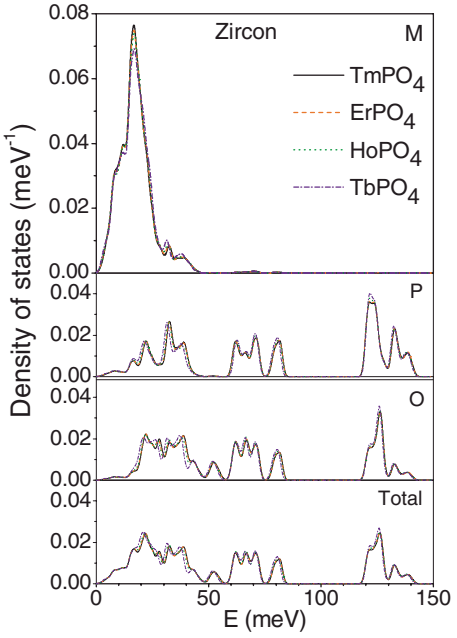

FIG. 3. (Color online) The calculated partial densities of states of the orthophosphates in their zircon phase.

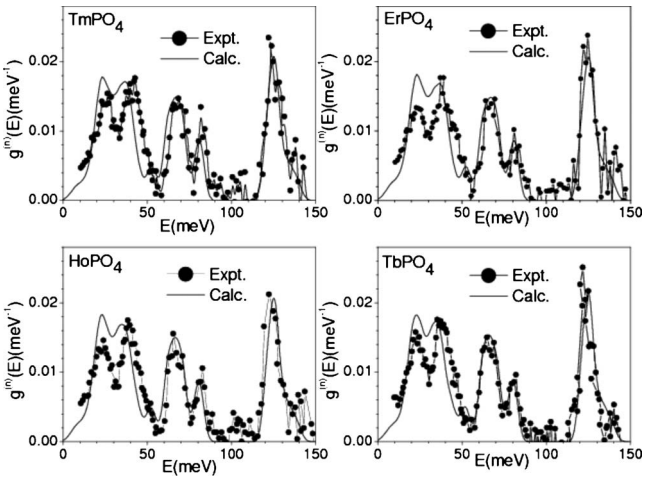

FIG. 4. Comparison between the experimental (T=300 K) and calculated (T=0 K) neutron-weighted phonon densities of states in the zircon phase of RPO_4 (R=Tm, Er, Ho, and Tb).

$$g^{n}(E) = B\sum_{k}\left\{\frac{4\pi b_k^2}{m_k}\right\} g_k(E), \tag{3}$$

where B is the normalization constant and b_k, m_k, and $g_k(I)$ are neutron coherent scattering length, mass and partial density of states of the kth atom in the unit cell, respectively. The weight factors in barns/atomic mass unit used in our calculation for various atoms are: Tm=0.038, Er=0.052,

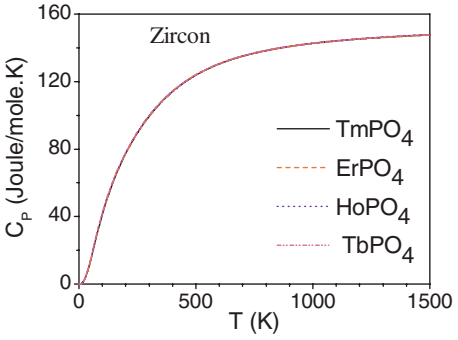

FIG. 5. (Color online) The calculated specific heat in the ambient pressure phase of RPO_4 (R=Tm, Er, Ho, and Tb) at P=0.

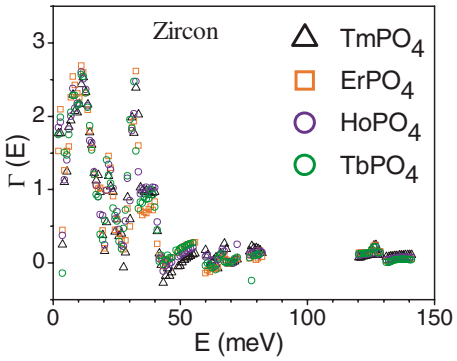

FIG. 6. (Color online) The calculated Grüneisen parameter as a function of RPO_4 (R=Tm, Er, Ho, and Tb) at P=0.

Ho=0.051, Tb=0.043, P=0.107, and O=0.265. The values of the neutron-scattering lengths of various atoms can be found from standard references.[31,35] The calculated neutron-weighted one phonon density of states (Fig. 4) are in good agreement with our measured data on RPO_4 (R=Tm, Er, Ho, and Tb). The spectra consist of phonon bands centered at about 24, 40, 68, 83, and 125 meV. There is a band gap in the energy range of 90–115 meV. The total phonon densities of states for RPO_4 are very similar due to the fact that the compounds are isostructural and the masses of the rare-earth atoms (R=Tm, Er, Ho, and Tb) are nearly same.

B. Thermodynamic properties

The calculated phonon density of states (Fig. 3) is used for the calculation of various thermodynamic properties such as the lattice specific heat, Grüneisen constant, thermal expansion, etc. in the zircon phase of $TmPO_4$, $ErPO_4$, $HoPO_4$, and $TbPO_4$. The temperature dependence of the specific heat (Fig. 5) exhibits the same profile for all the members in this study.

The calculation of thermal expansion is carried out under quasiharmonic approximation. Each mode contributes to volume thermal expansion[29] equal to $\alpha_V = \frac{1}{BV}\Sigma_i \Gamma_i C_{Vi}(T)$, where, $\Gamma_i (= -\partial \ln E_i / \partial \ln V)$ and C_{Vi} are the mode Grüneisen parameter and specific heat, respectively, of the phonons in the ith state. The calculated pressure dependence of phonon modes is used for the calculation of energy dependence of Grüneisen parameter $\Gamma(E)$ (Fig. 6), which in turn is used for the calculation of thermal expansion (Fig. 7) using the relation given above. The band gap from about 85 to 115 meV in the density of states appears also in the Grüneisen parameter plot.

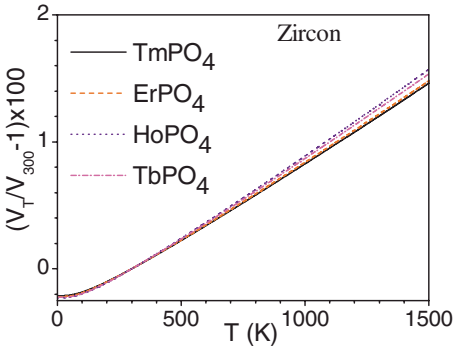

FIG. 7. (Color online) The calculated thermal-expansion behavior of RPO_4 (R=Tm, Er, Ho, and Tb) at P=0.

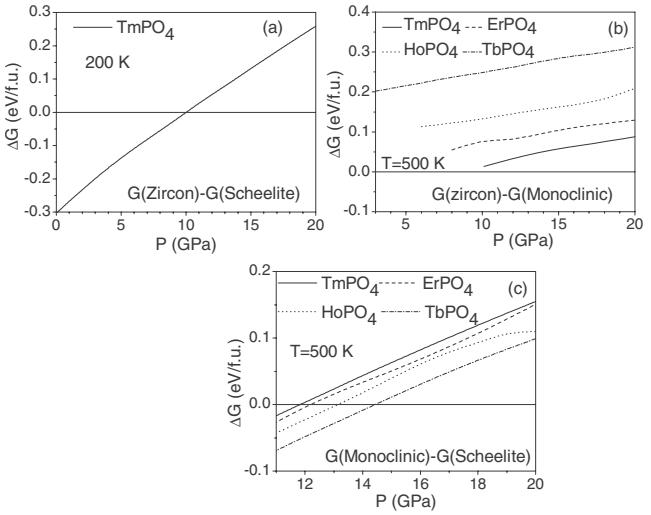

FIG. 8. Typical plots of the differences in the free energies of competing phases in RPO_4 (R=Tm, Er, Ho, and Tb) as a function of pressure.

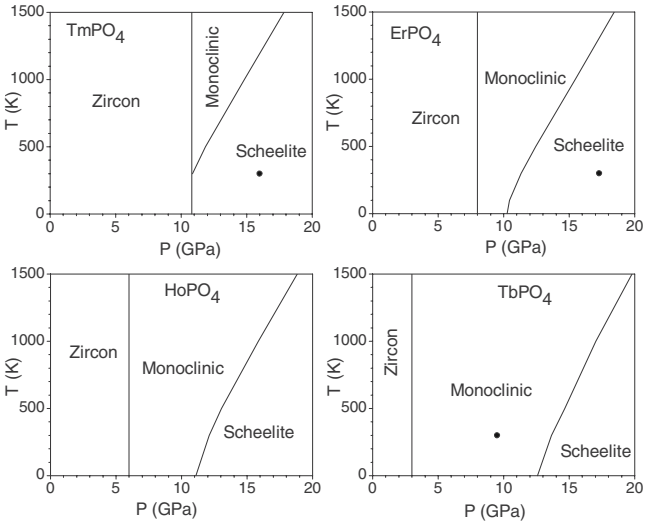

FIG. 9. The calculated phase diagrams of $TmPO_4$, $ErPO_4$, $HoPO_4$, and $TbPO_4$ and as obtained from the free-energy calculations. The experimental data for $ErPO_4$ and $TmPO_4$ are taken from Ref. 36 while the datum for $TbPO_4$ is from Ref. 24. The transition to monoclinic phase in $TmPO_4$, $ErPO_4$, and $TbPO_4$ is calculated at 10.8 GPa, 8 GPa, and 3 GPa, respectively, above 300 K. Experimentally the transition in these compounds at ambient temperature is observed on compression at 16 GPa, 17.2 GPa, and 9.5 GPa, respectively, and might have involved some hysteresis. Zircon, monoclinic and scheelite in the figure indicate the calculated phase stability regions for RPO_4 (R=Tm, Er, Ho, and Tb). $TmPO_4$ on compression goes directly from zircon-to-scheelite structure below 300 K while it goes from zircon-to-monoclinic and then to scheelite structures above 300 K.

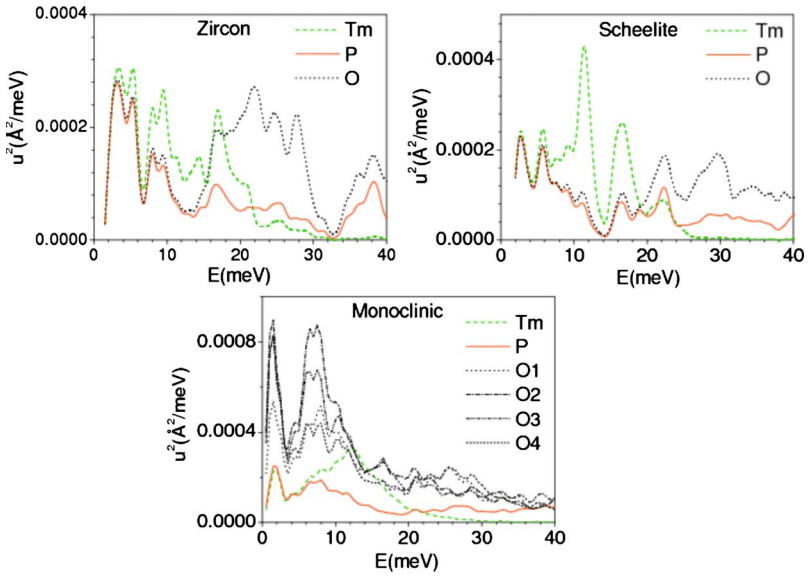

FIG. 10. (Color online) Mean-square amplitudes of various atoms arising from the phonons of energy E (integrated over the Brillouin zone) at $T=300$ K and $P=11$ GPa in various phases of $TmPO_4$.

C. Free energy and phase diagram

Zircon-structured rare-earth phosphates are known to transform to monoclinic or scheelite phase at high pressure. Monoclinic and scheelite phase transitions are known to be very competitive. Earlier we have reported lattice-dynamical calculations for the zircon-structured natural silicates,[27] $MSiO_4$ (M=Zr, Hf, Th, and U), where the thorium compound with the largest ionic radius at the M site shows transition to monoclinic phase at high pressure while other compounds (M=Zr, Hf, and U) transform to the scheelite phase. For the rare-earth compounds RPO_4 (R=Tm, Er, Ho, and Tb), Tm has the smallest ionic radii among the four rare-earth atoms. So initially we started with the calculations for $TmPO_4$. The zircon-to-monoclinic phase transition has been experimentally observed[36] in $TmPO_4$ at 16 GPa and ambient temperature. So we have chosen a value of the radius parameter of Tm atom such that the model produces a dynamically stable monoclinic phase at high pressure. For the radius parameter R(Tm)=2.110 Å, our calculation for the monoclinic phase at 0 K shows unstable phonon modes below 10.8 GPa and stable phonons above that pressure. Because of this we have not shown the free-energy difference [Fig. 8(b)] below this critical pressure and abscissa in Fig. 8(b) does not go down to zero.

As mentioned in Sec. III we have included vibrational entropy while calculating the free energies. We find that at pressures above 10.8 GPa and temperatures above 300 K, the monoclinic phase has lower free energy as compared to the zircon phase, and the phonon modes are also stable. The transition to monoclinic phase is therefore expected at this critical pressure and shown in Fig. 9 accordingly. Thus, phase transition in $TmPO_4$ is calculated at 10.8 GPa which has been experimentally[36] observed at 16 GPa and might have involved some hysteresis. The experiment does not show any further phase transition up to 25 GPa. However, our free-energy calculation shows that the monoclinic phase further transforms to the scheelite phase at higher pressure above 300 K (Fig. 9).

Further, the free-energy calculations have been used for obtaining the phase diagram (Fig. 9) of $TmPO_4$ over a wide range of pressure and temperature. $TmPO_4$ on compression goes from "zircon-to-monoclinic and then to scheelite" structures above 300 K; however, it goes directly from "zircon-to-scheelite" structure below 300 K.

The radius parameter in the short-ranged part of the potential is related to the ionic radius. Shannon[37] ionic radii of Tm, Er, Ho, and Tb atoms are 0.994 Å, 1.004 Å, 1.015 Å, and 1.04 Å, respectively. The radii parameters of the rest of the rare-earth atoms (Er, Ho, and Tb) in other compounds were obtained by scaling the ionic radii of R (Er, Ho, and Tb) atoms to the ratio of the radius parameter and ionic radius of Tm atom in octahedral coordination. The values of the scaled radii parameters are: R(Tm)=2.110 Å, R(Er)=2.130 Å, R(Ho)=2.155 Å, and R(Tb)=2.208 Å. The calculated phase diagrams of various lanthanide orthophosphates, RPO_4 as shown in Fig. 8 indicate phase transition as found in the experiments.[24,36] *Ab initio* total-energy calculations for

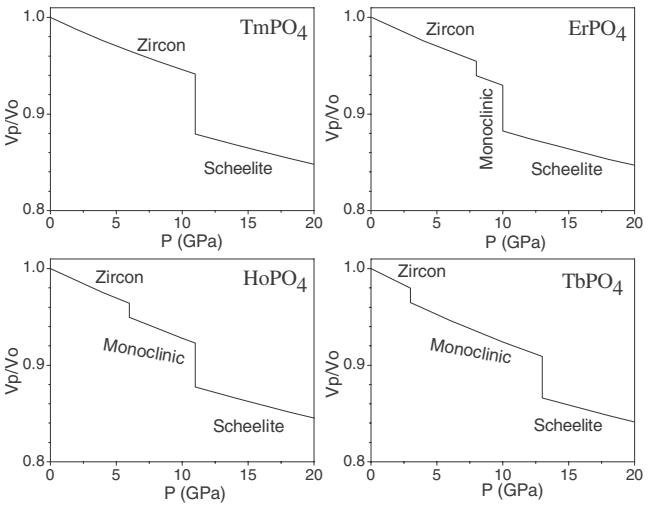

FIG. 11. The calculated equation of state of RPO_4 (R=Tm, Er, Ho, and Tb) at T=0. For $TmPO_4$, our calculations show zircon-to-scheelite transitions at 0 K. For the rest of the compounds we observe zircon-monoclinic-scheelite transition as a function of pressure at 0 K.

TABLE II. The elastic constants and bulk modulus in zircon phase (at $P=0$ GPa and $T=0$ K) of $ErPO_4$, $HoPO_4$, $TbPO_4$, and $TmPO_4$ (in GPa units). The experimental values are at ambient pressure and room temperature.

Elastic constant	Calc. $TmPO_4$ (zircon)	Calc. $ErPO_4$ (zircon)	Calc. $HoPO_4$ (zircon)	Calc. $TbPO_4$ (zircon)
C_{11}	275	270	265	251
C_{33}	411	407	401	388
C_{44}	81	79	77	72
C_{66}	10	9	7	4
C_{12}	40	38	36	33
C_{13}	136	134	130	124
$B_{(calc.)}$	176	174	170	161
B	147.2[b]	168[a]	143.4[b]	138.8[b]

[a]Expt. (Ref. 28).
[b]Theory (Ref. 12).

$TbPO_4$ (Ref. 38) also indicate a similar structural phase transition at about 9.6 GPa. The experimental datum of the transition pressure is not available for $HoPO_4$. However, as the ionic radius of Ho lies between those of Er and Tb atom, zircon-structured $HoPO_4$ is also expected to transform to monoclinic phase as seen in our calculations. The potential reproduces well the observed atomic lattice parameters and fractional atomic coordinates in the zircon phase (Table I).

Figure 8 shows typical plots of the differences in the free energies of competing phases as a function of pressure for all RPO_4 compound under study. We find that the monoclinic phase is stabilized compared to the zircon phase [Fig. 8(b)] at comparatively lower pressures when the radius of the R atom is larger. However, the scheelite phase is stabilized over the monoclinic phase [Fig. 8(c)] at a higher pressure in case of larger R atom. The free-energy difference plot for zircon-to-scheelite phase transition [Fig. 8(a)] in $TmPO_4$ is also calculated at 200 K.

In order to understand the nature of phase transition in RPO_4, we have plotted $\langle u^2 \rangle$ (Fig. 10) of atoms for $TmPO_4$ in various phases. We will concentrate on the low-energy phonon modes since these modes are believed to be responsible for phase transitions in these compounds. We observe that in the zircon and scheelite phases the low-energy modes up to 5 meV involve equal amplitude of various atoms. These modes are largely acoustic in nature. For 5–20 meV, the calculated $\langle u^2 \rangle$ values of P and O atoms are nearly the same which indicates translation of PO_4 tetrahedra as a whole. On the other hand, in the monoclinic phase, the low-energy modes up to 10 meV involve smaller amplitudes of Tm and P atoms in comparison to O atoms, indicating simultaneous rotation and translation of PO_4 and TmO_8. Further, the various oxygen atoms constituting the PO_4 tetrahedra in the monoclinic phase have significantly different values of their vibrational amplitudes, indicating distortions of the PO_4 tetrahedra. The presence of low-energy libration of PO_4 and TmO_8 polyhedra in the monoclinic phase seems to play a key role for the zircon-to-monoclinic phase transition. However, the librational modes in the zircon and scheelite phases occur above 20 meV. Further, the comparison of $\langle u^2 \rangle$ of various atoms in various phases at low energies shows that the absolute values of $\langle u^2 \rangle$ for Tm and P atoms are nearly same in all the phases. However, in the monoclinic phase the absolute value of $\langle u^2 \rangle$ for oxygen atoms is very high compared to that in the zircon and scheelite phases. This may be primarily due to shift of the oxygen vibrations at low energies which, in turn, result in low-energy librational modes in the monoclinic phase.

The calculated equations of state are shown in Fig. 11 for the ambient and high-pressure phases. The structure of the high-pressure phases are obtained by minimization of Gibbs free energy with respect to the structure variables while keeping the space group unchanged. The experimental data[36] of equation of state for $ErPO_4$ shows 4% volume drop at the zircon-to-monoclinic phase transition while our calculations show 1.5% drop in volume. The bulk modulus values (experimental[36] and calculated[19]) are compared with our calculated bulk modulus values. As seen from Table II the bulk modulus values are over estimated by our calculation.

VI. CONCLUSIONS

Inelastic neutron-scattering measurements of the phonon density of states carried out on polycrystalline samples of RPO_4 (R=Tm, Er, Ho, and Tb), in the zircon phase are in good agreement with our lattice-dynamics calculations. The calculated free energies show that zircon is the stable structure of RPO_4 at low pressures and at ambient temperature, and a transformation to an intermediate monoclinic phase occurs on compression, followed by the formation of the scheelite structure at higher pressures. The good agreement between various calculated and experimental dynamical properties indicates that our interatomic potential model is reasonable. The calculated free energies in various phases of RPO_4 show that stability of intermediate monoclinic phase is determined by the ionic size of the R atom.

ACKNOWLEDGMENTS

Works performed at Argonne and Oak Ridge National Laboratory is supported by the U.S. DOE-BES under Contract No. W-31-109-ENG-38 and by the Division of Materials Sciences and Engineering, Office of Basic Energy Sciences, U.S. Department of Energy, respectively.

[1] R. C. Ewing, Science **192**, 1336 (1976).
[2] H. Matzke, V. V. Rondinella, and T. Wiss, J. Nucl. Mater. **274**, 47 (1999).
[3] T. Norby and N. Christiansen, Solid State Ionics **77**, 240 (1995).
[4] D. B. Marshall, P. E. Morgan, and R. M. Housley, J. Am. Ceram. Soc. **80**, 677 (1997).
[5] L. A. Boatner, G. W. Beall, M. M. Abraham, C. B. Finch, P. G. Huray, and M. Rappaz, in *The Scientific Basis for Nuclear Waste Management*, edited by C. J. Northrup (Plenum Press, New York, 1980), Vol. II, p. 289.
[6] A. Rapaport, O. Moteau, M. Bass, L. A. Boatner, and C. Deka, J. Opt. Soc. Am. B **16**, 911 (1999).
[7] C.-K. Loong, M. Loewenhaupt, J. C. Nipko, M. Braden, and L. A. Boatner, Phys. Rev. B **60**, R12549 (1999).
[8] J. C. Nipko, C.-K. Loong, M. Loewenhaupt, M. Braden, W. Reichart, and L. A. Boatner, Phys. Rev. B **56**, 11584 (1997).
[9] R. Mittal, S. L. Chaplot, N. Choudhury, and C.-K. Loong, J. Phys.: Condens. Matter **19**, 446202 (2007).
[10] K. Kompe, H. Borchert, J. Storz, A. Lobo, S. Adam, T. Moller, and M. Haase, Angew. Chem., Int. Ed. **42**, 5513 (2003).
[11] S. V. Ushakov, K. B. Helean, A. Navrotsky, and L. A. Boatner, J. Mater. Res. **16**, 2623 (2001).
[12] S. Y. Zhang, F. M. Gao, and C. X. Wu, J. Alloys Compd. **275**, 835 (1998).
[13] Y. Hikichi, T. Ota, K. Daimon, T. Hattori, and M. Mizuno, J. Am. Ceram. Soc. **81**, 2216 (1998).
[14] L. Perrière, D. Bregiroux, B. Naitali, F. Audubert, E. Champion, D. S. Smith, and D. Bernache-Assollant, J. Eur. Ceram. Soc. **27**, 3207 (2007).
[15] A. Meldrum, L. A. Boatner, and R. C. Ewing, Phys. Rev. B **56**, 13805 (1997).
[16] A. Meldrum, S. J. Zinkle, L. A. Boatner, and R. C. Ewing, Phys. Rev. B **59**, 3981 (1999).
[17] S. Zhang, S. Zhou, H. Li, and L. Li, Inorg. Chem. **47**, 7863 (2008).
[18] H. L. Li, S. H. Zhou, and S. Y. Zhang, J. Solid State Chem. **180**, 589 (2007).
[19] H. Li, S. Zhang, S. Zhou, and X. Cao, Inorg. Chem. **48**, 4542 (2009).
[20] G. M. Begun, G. W. Beall, L. A. Boatner, and W. J. Gregor, J. Raman Spectrosc. **11**, 273 (1981).
[21] X. Wang, I. Loa, K. Syassen, M. Hanfland, and B. Ferrand, Phys. Rev. B **70**, 064109 (2004).
[22] F. X. Zhang, J. W. Wang, M. Lang, J. M. Zhang, and R. C. Ewing, Phys. Rev. B **80**, 184114 (2009).
[23] F. X. Zhang, M. Lang, R. C. Ewing, J. Lian, Z. W. Wang, J. Hu, and L. A. Boatner, J. Solid State Chem. **181**, 2633 (2008).
[24] A. Tatsi, E. Stavrou, Y. C. Boulmetis, A. G. Kontos, Y. S. Raptis, and C. Raptis, J. Phys.: Condens. Matter **20**, 425216 (2008).
[25] R. Mittal, A. B. Garg, V. Vijayakumar, S. N. Achary, A. K. Tyagi, B. KGodwal, E. Busetto, A. Lausi, and S. L. Chaplot, J. Phys.: Condens. Matter **20**, 075223 (2008).
[26] S. L. Chaplot, L. Pintschovius, N. Choudhury, and R. Mitttal, Phys. Rev. B **73**, 094308 (2006).
[27] P. P. Bose, R. Mittal, and S. L. Chaplot, Phys. Rev. B **79**, 174301 (2009).
[28] M. Rappaz, L. A. Boatner, and M. M. Abraham, J. Chem. Phys. **73**, 1095 (1980).
[29] G. Venkatraman, L. Feldkamp, and V. C. Sahni, *Dynamics of Perfect Crystals* (MIT, Cambridge, 1975).
[30] P. Bruesch, *Phonons: Theory and Experiment* (Springer, New York, 1982), Vols. 1-2.
[31] www.ncnr.nist.gov; V. F. Sears, Neutron News **3**, 26 (1992).
[32] W. O. Milligan, D. F. Mullica, G. W. Beall, and L. A. Boatner, Acta Crystallogr., Sect. C: Cryst. Struct. Commun. **C39**, 23 (1983).
[33] S. Skanthakumar, C.-K. Loong, L. Soderholm, J. Nipko, J. W. Richardson. Jr., M. M. Abraham, and L. A. Boatner, J. Alloys Compd. **225**, 595 (1995).
[34] J. N. Lee and H. W. Moos, Phys. Rev. B **5**, 3645 (1972).
[35] *Neutron Data Booklet*, edited by A.-J. Dianoux and G. Lander (Institut Laue-Langevin, Grenoble, France, 2002).
[36] R. Lacomba-Perales, D. Errandonea, Y. Meng, and M. Bettinelli, Phys. Rev. B **81**, 064113 (2010).
[37] http:\\abulafia.mt.ic.ac.uk\shannon\ptable.php
[38] J. López-Solano, P. Rodríguez-Hernández, A. Muñoz, O. Gomis, D. Santamaría-Perez, D. Errandonea, F. J. Manjón, R. S. Kumar, E. Stavrou, and C. Raptis, Phys. Rev. B **81**, 144126 (2010).